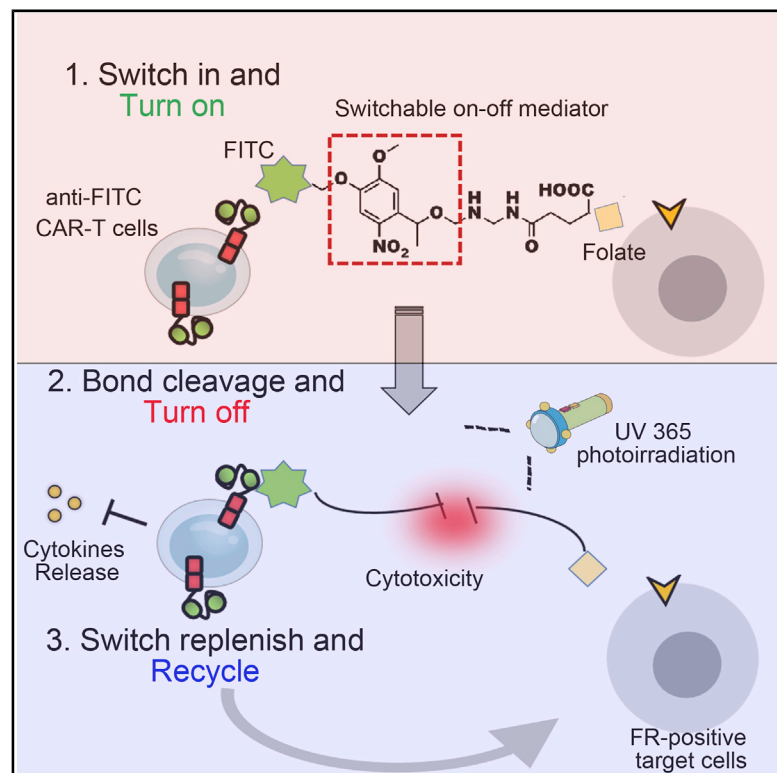


Cell Chemical Biology

Photoswitchable CAR-T Cell Function *In Vitro* and *In Vivo* via a Cleavable Mediator

Graphical Abstract



Authors

Bo Zhang, Yan Wang, Shenlong Huang, ..., Demin Zhou, Lingjun Li, Xuan Zhang

Correspondence

deminzhou@bjmu.edu.cn (D.Z.), lingjunlee@aliyun.com (L.L.), zxpumch2003@sina.com (X.Z.)

In Brief

CAR-T is a powerful technology for cancer therapy, but is largely limited by inherent controllability issues. Zhang et al. developed an accurate controllable approach based on the bond-cleavage chemistry combined with universal anti-FITC CAR-T cells, allowing the regulation of CAR-T cells in a switchable manner.

Highlights

- Folate-O-FITC switch CAR-T cells to an activated state in a dose-dependent manner
- CAR-T-induced cytotoxicity can be rapidly terminated by the cleavage of folate-O-FITC
- CAR-T can be turned on/off on demand by supplementation/cleavage of folate-O-FITC
- Such switchable regulated manner would not compromise antitumor effects of CAR-T cells

Article

Photoswitchable CAR-T Cell Function *In Vitro* and *In Vivo* via a Cleavable Mediator

Bo Zhang,^{1,2,3,6} Yan Wang,^{2,6} Shenlong Huang,^{4,6} Jiaqi Sun,² Min Wang,^{3,5} Wenxiao Ma,² Yanbo You,⁴ Ling Wu,² Jin Hu,^{1,3} Wei Song,¹ Xudong Liu,¹ Shengjie Li,¹ Hua Chen,^{3,5} Guisheng Zhang,⁴ Lihe Zhang,² Demin Zhou,^{2,*} Lingjun Li,^{4,*} and Xuan Zhang^{3,5,7,*}

¹Department of Medical Research Center, Peking Union Medical College Hospital, Chinese Academy of Medical Sciences and Peking Union Medical College, Beijing 100730, China

²State Key Laboratory of Natural and Biomimetic Drugs, School of Pharmaceutical Sciences, Peking University, Beijing 100191, China

³Clinical Immunology Center & Epigenetics Center, Chinese Academy of Medical Sciences and Peking Union Medical College, Beijing 100730, China

⁴Henan Key Laboratory of Organic Functional Molecule and Drug Innovation, School of Chemistry and Chemical Engineering Henan Normal University, Xinxiang, Henan 453007, China

⁵Department of Rheumatology and Clinical Immunology, Peking Union Medical College Hospital, Chinese Academy of Medical Sciences and Peking Union Medical College, Beijing 100730, China

⁶These authors contributed equally

⁷Lead Contact

*Correspondence: deminzhou@bjmu.edu.cn (D.Z.), lingjunlee@aliyun.com (L.L.), zxpumch2003@sina.com (X.Z.)

<https://doi.org/10.1016/j.chembiol.2020.10.004>

SUMMARY

Chimeric antigen receptor (CAR)-T-based therapeutics are a breakthrough in cancer treatment; however, they are hampered by constitutive activation, which leads to worrisome side effects. Engineering CAR-T cells to be as tightly controllable as possible remains a topic of ongoing investigation. Here, we report a photo-switchable approach that uses a mediator for the at-will regulation of CAR-T cells. This mediator carries dual folate and fluorescein isothiocyanate moieties tethered by an ortho-nitrobenzyl ester photocleavable linker. CAR-T cells were shown to be highly cytotoxic to targeted cells only in the presence of the mediator and acted in a dose-dependent manner. The toxicity of CAR-T cells can be rapidly terminated by cleavage of the mediator, and the effects of CAR-T cells can be activated again by resupplementation with the mediator without compromising tumor therapy. The approach described here provides a direction for enhancing the controllability of CAR-T cells and can likely be applied in other immunotherapies.

INTRODUCTION

Immunotherapy has emerged as a potential approach for the treatment of cancer, with chimeric antigen receptor (CAR)-T cells already in use in the clinic (Grupp, et al., 2013). The premise of CAR-T cells is the genetic modification of T cells to express a CAR for the recognition of tumor surface antigens specific to an individual patient. After infusion into a patient, CAR-T cells become activated upon contact with their targeted antigen and proceed to proliferate and destroy cancer cells. CAR-T cells become cytotoxic through several mechanisms, including extensive cell proliferation, increasing the degree to which the cells are toxic to other living cells and, more importantly, causing the increased secretion of cellular factors, such as cytokines, interleukins, and growth factors (Barrett, et al., 2014; Grupp, et al., 2013). In the human body, a population of CAR-T cells expands by 100- to 10,000-fold in response to their antigen, making the magnitude of their toxicity unpredictable and difficult to manage. These adverse reactions, including cytokine release syndrome (CRS), are worrisome and sometimes fatal due to either on-target, off-tumor reactions against healthy tissue or excessive

on-target, on-tumor reactions against heavy tumor loads (Acharya, et al., 2019; Brudno and Kochenderfer, 2016). Ironically, CRS is considered an “on-target” effect, in that its presence demonstrates that active T cells are at work in the body (Brudno and Kochenderfer, 2016).

Although how CAR-T cells work is understood, translation of this knowledge to the management of serious CRS is ongoing. Numerous approaches have been implemented to address this problem, such as neutralizing inflammatory cytokines by antagonist proteins (Giavridis, et al., 2018; Kotch, et al., 2019; Norelli, et al., 2018), inducing CAR-T cell death by incorporating suicide genes (Di Stasi, et al., 2011; Straathof, et al., 2005), and applying bifunctional mediators to bridge CAR-T cells and target cells (Cao, et al., 2016; Kim, et al., 2015; Tamada, et al., 2012; Urbanska, et al., 2012). Despite the promise of these approaches, achieving immediate and complete control of the toxicity of CAR-T cells is still challenging considering the time-consuming procedures required for bispecific adaptors based on metabolism (Lee, et al., 2019); furthermore, antibodies can only be locked to known cytokines, which may not be sufficiently comprehensive. As recent chemical developments have focused on

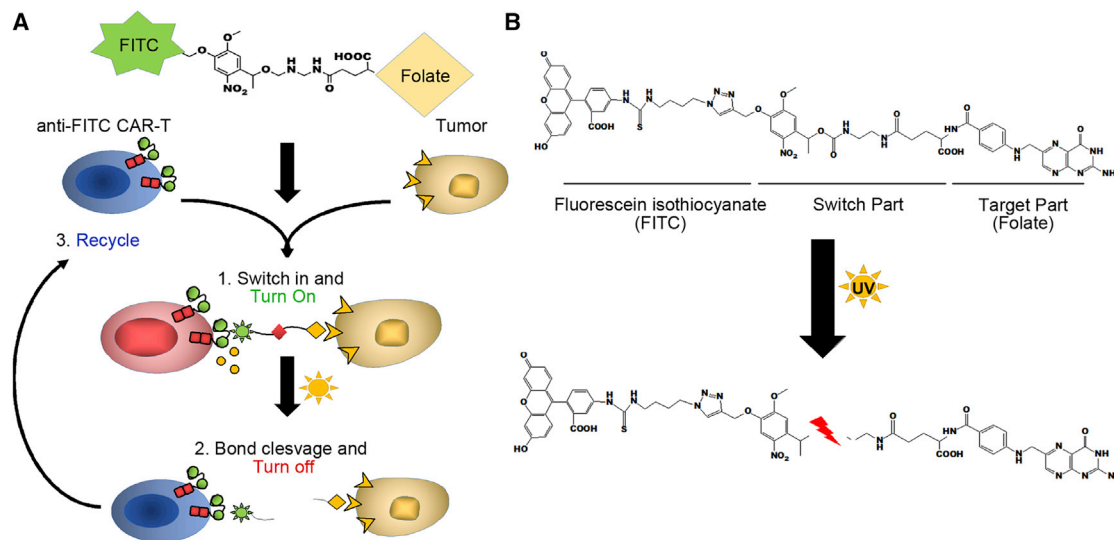


Figure 1. Schematic Representation of a Photoswitchable CAR-T Cell System Based on a Cleavable Mediator

(A) Photoswitchable CAR-T cell system based on a cleavable mediator.

(B) Structure of the photocleavable mediator folate-O-FITC in which the FITC and folate moieties are tethered together via a photosensitive ortho-nitrobenzyl ester.

“bond-cleavage” reactions with excellent characteristics in the spatial and temporal regulation of biological functions (Li and Chen, 2016; Oliveira, et al., 2020; Tomlin, et al., 2018; Wang, et al., 2019), it is thus becoming possible to further enhance the controllability of CAR-T cells in a potentially switchable manner.

As a proof of concept, here, we report a photoswitchable approach using the well-known mediator folate-fluorescein isothiocyanate (FITC) (Figure 1A) (Kim, et al., 2015), but its conventional tether was replaced with a photocleavable linker (Figure 1B) (Klan, et al., 2013) to render CAR-T cells as controllable as possible. This system includes three key steps: (1) activation of inert CAR-T cells through a mediator, which carries folate and fluorescein isothiocyanate moieties tethered by an ortho-nitrobenzyl linker (folate-O-FITC), for binding CAR-T cells and target cells, respectively; (2) termination of the toxic effects of CAR-T cells via photoirradiation that rapidly breaks down the linker of folate-O-FITC; and (3) reactivation of CAR-T cells by supplementation with the mediator as needed.

We find that folate-O-FITC has the ability to switch inert CAR-T cells to an activated state, and the persistence of the mediator forces CAR-T cells to remain in the active state. With exposure to light pulses at nondetrimental wavelengths, CAR-T cells are switched off following breakdown of the mediator and can be switched on again by resupplementation with the mediator. The versatile approach described here may provide a direction for enhancing the controllability of CAR-T cells and can likely be applied in other immunotherapies.

RESULTS

Generation and Characterization of Folate-O-FITC Mediator and Anti-FITC CAR-T Cells

We first synthesized the folate-O-FITC mediator based on a modular assembly (Chang, et al., 2016; Jung, et al., 2010; Ka-

neko, et al., 2011; Menard-Moyon, et al., 2015; Sarfaty, et al., 2018; Tan, et al., 2009; Tso, et al., 2016) (Figure S1A). In brief, the ortho-nitrobenzyl ester bearing a terminal alkyne and free amine group was obtained by propargylation, ester exchange, and ammonolysis from a commercial ortho-nitrobenzyl alcohol. Coupling of the ortho-nitrobenzyl ester to folate was conducted with dicyclohexylcarbo-diimide as the condensing reagent, and conjugation to FITC was then completed using the CuAAC reaction. The structure and purity of folate-O-FITC were verified by MALDI-TOF-MS and nuclear magnetic resonance (Figure S1B), and their photosensitivity was confirmed by UV365 irradiation.

To create a FITC-specific CAR, the anti-FITC scFv clone 4M5.3 (Midelfort, et al., 2004; Vaughan, et al., 1996) was subcloned into a lentiviral vector (Figure S2A) and then transduced into human T cells as described previously (Kim, et al., 2015; Ma, et al., 2016). The transduction efficiency was ~90%, as measured by flow cytometry (Figure S2B). Proper scFv folding on the T cell surface was verified by staining CAR-T cells with anti-mouse IgG F(ab')₂-APC and the mediator (FITC) simultaneously. We observed that nearly all T cells expressing the scFv bound FITC (~50%), which was a significantly higher level of binding than that observed in nontransduced T cells (Figure S2C), indicating that the scFv expressed on the cellular surface was solvent exposed and accessible to the FITC ligand.

Activation of Anti-FITC CAR-T Cells by Folate-O-FITC *In Vitro*

Next, we evaluated the ability of folate-O-FITC to direct inert anti-FITC CAR-T cells to bind to folate receptor (FR)-positive KB cells using a cytotoxicity assay with FR-negative A549 cells as a negative control (Kim, et al., 2015). We found that either at an effector:target cell (E:T) ratio of 3:1 or 10:1, folate-O-FITC demonstrated high potency in directing anti-FITC CAR-T cells to kill KB

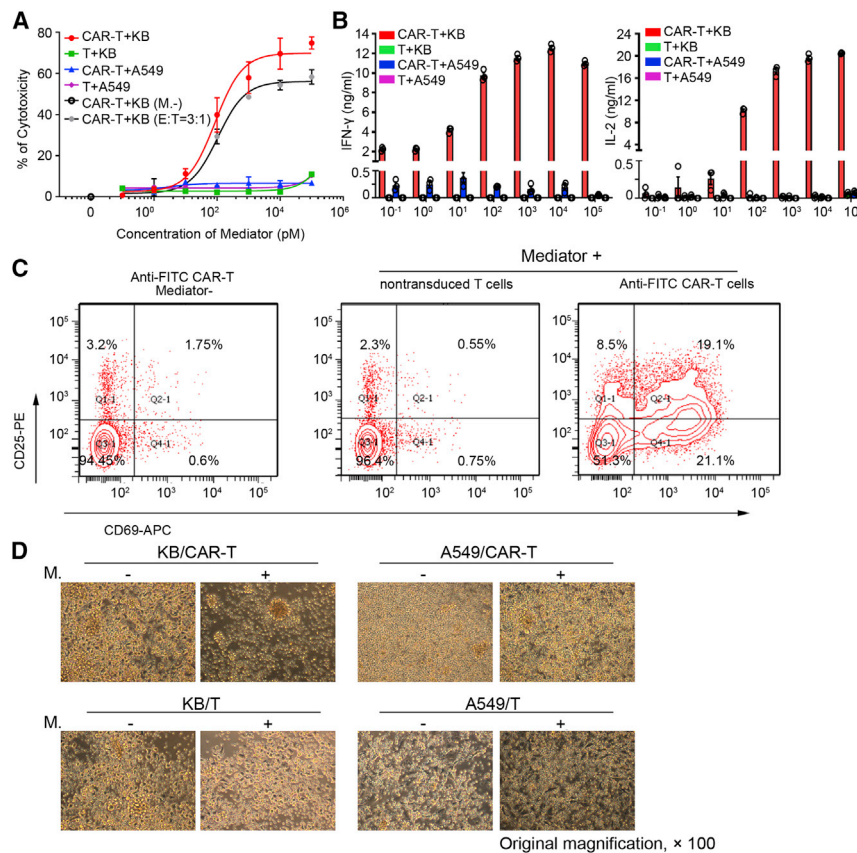


Figure 2. Characterization of Folate-O-FITC-Mediated Activation of Anti-FITC CAR-T Cells *In Vitro*

(A) Dose-dependent activation of CAR-T cells by folate-O-FITC. The cytotoxicity of CAR-T cells induced by the mediator were measured by incubation of anti-FITC CAR-T cells and FR-positive KB cells at a ratio of either 3:1 or 10:1, and the amount of LDH released into the culture medium detected. The KB cells cultured with nontransduced T cells and the FR-negative A549 cultured group were applied as negative control. The percentage cytotoxicity was defined as the percentage of (experimental – effector spontaneous – target spontaneous)/(target maximum – target spontaneous), where “effector” means CAR-T cells or nontransduced control T cells, and “target” means KB or A549 cells, respectively. The data are presented as the mean ± SEM derived from triplicate samples (n = 3).

(B) Quantification of cytokine (IFN-γ and IL-2) levels in the cultures described in (A) by ELISA. Data are presented as the mean ± SEM derived from triplicate samples (n = 3).

(C) Characterization of folate-O-FITC-mediated activation of CAR-T cells by flow cytometry analysis of CD25 and CD69 expression on CAR-T cells. CAR-T cells were cocultured with KB cells either in the presence or absence of the mediator for 24 h with nontransduced T cells as a control.

(D) Morphological features of folate-O-FITC-dependent CAR-T cell aggregates. All images were acquired from the center field of each well and are shown at 100× magnification. For (C) and (D), representative results from one of three experiments are shown.

cells over 24 h (half maximal effective concentration = 109.5 ± 28.86 or 93.2 ± 12.65 pM for E:T = 3:1 or 10:1, respectively, [Figure 2A](#)). In contrast, the mediator failed to induce the lysis of KB cells by nontransduced T cells. No significant cytotoxicity was observed with A549 cells and either anti-FITC CAR-T cells or nontransduced T cells, demonstrating the high selectivity of folate-O-FITC for the activation of anti-FITC CAR-T cells. Consistent with these results, increased secretion of cellular factors was detected during this 24-h assay, and the levels of the cytokines, interferon γ (IFN-γ) and interleukin-2 (IL-2), were positively correlated with the concentration of folate-O-FITC only in the case of FR-positive cells ([Figure 2B](#)). The binding affinity and cytotoxicity of the mediator were also compared with those of its parental folate-FITC; nonsignificant differences were observed, indicating that the installed nitrobenzyl linker has little effect on these functions ([Figures S3A and S3B](#)).

The activation of CAR-T cells by the mediator was further tested by monitoring the activation markers and, as anticipated, folate-O-FITC significantly increased the CD25 and CD69 expression levels of anti-FITC CAR-T cells compared with those of nontransduced T cells only in the presence of FR-positive cells ([Figure 2C](#)). In addition, the selective formation of aggregates, indicative of crosslinking between T cells and target cells, was visible only in cocultures of anti-FITC CAR-T and KB cells with the mediator but not in any of the controls ([Figure 2D](#)). Clearly, supplementation with the mediator switches inert CAR-T cells

to an activated state, and persistence of the mediator in the medium forces CAR-T cells to remain in this activated state.

Inactivation of CAR-T Cells by Photoirradiation and Reactivation by Supplementation with Folate-O-FITC

To explore whether the activated anti-FITC CAR-T cells could be silenced by photoirradiation, we first tested the capacity of irradiation to promote the detachment of CAR-T cells from KB cells. As described above, anti-CD3-APC-labeled CAR-T cells and anti-FR-PE-labeled KB cells were cocultured at a 1:1 ratio for 1 h at 4°C. The percentage of PE/APC double-positive cells was significantly greater in the presence of the mediator, as shown in [Figure 3A](#), than in the absence of the mediator. We then irradiated half of the experimental cells at 365 nm, with the remaining cells serving as a negative control. We found that, upon irradiation for 5 min, the percentage of double-positive cells sharply decreased to the level in the nonirradiated group, suggesting that the ortho-nitrobenzyl linker within the mediator was effectively broken. A parallel experiment by detection of photoirradiated Jurkat or KB cells labeled with corresponding fluorescent antibody was also performed, and no obvious decrease of fluorescent intensity was found even when the duration of photoirradiation was up to 15 min, suggesting that the decrease of the double-positive cell was indeed ascribed to the detachment of Jurkat and KB cells ([Figure S4A](#)). Notably, analysis of cell clusters through fluorescence and

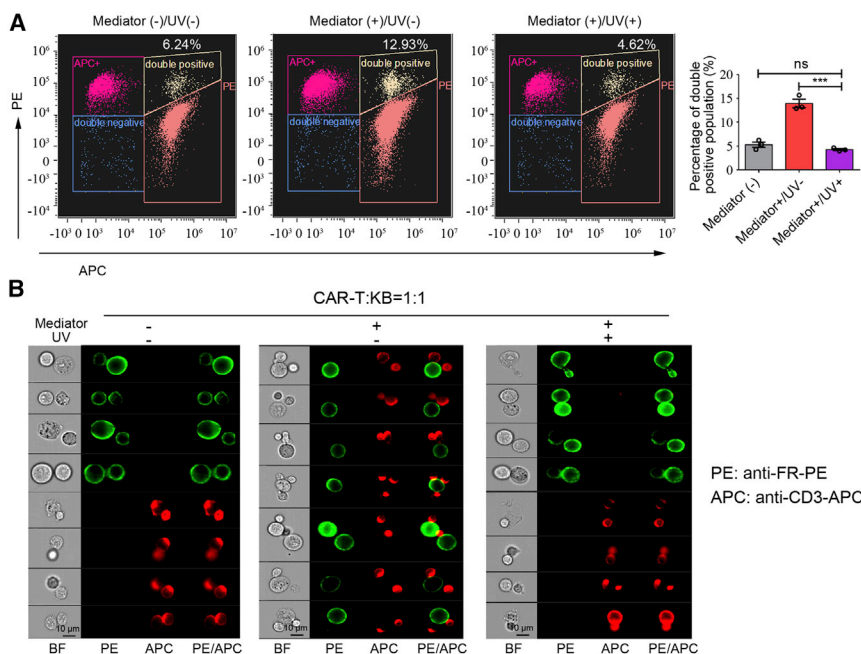


Figure 3. Characterization of Photoirradiation-Induced Detachment of CAR-T/KB Cell Clusters through Fluorescence Imaging

(A) Folate-O-FITC-mediated attachment and photoswitchable detachment of CAR-T cells and KB cells analyzed by flow cytometry in triplicate experiments. The data are presented as the mean \pm SEM of triplicate experiments ($n = 3$), and the p values shown were determined by two-tailed, unpaired Student's t tests; *** $p \leq 0.001$.

(B) Representative confocal fluorescence images of cell clusters with PE and APC double-staining images obtained by flow cytometry, as shown in (A). All images were acquired with a 40 \times objective, analyzed by IDEAS software, and illustrated in a channel series. The channels used for imaging were as follows: bright-field (BF, channel 1), PE (anti-FR-PE for KB cells, channel 2), and APC (anti-CD3-APC for CAR-T cells, channel 3). Scale bar, 10 μ m.

bright-field imaging showed that the cell clusters in the presence of the mediator were mostly composed of both KB and CAR-T cells at a ratio of 1:1 or 1:2, whereas the nonspecific self-adhesion of CAR-T cells and KB cells was predominant in the nonirradiated groups (Figure 3B). Optimization of the irradiation time indicated an increased degree of detachment with increasing irradiation time up to 10 min for CAR-T cells and up to 20 min for KB cells (Figure S4B). No significant decrease in cell viability was observed for either cell line, even with irradiation for as long as 30 min (Figure S4C).

Upon validating the feasibility of the mediator-induced detachment of CAR-T cells and target cells, we then designed a time course experiment (Figure 4A) to monitor the mediator-induced *in vitro* cytotoxicity and photoirradiation-mediated regulation. The coculture of CAR-T cells with KB cells in the presence of folate-O-FITC for 4 h led to marginal but detectable cytotoxicity, accompanied by mild IL-2 and IFN- γ release (Figure 4B). Then, some of the cultured cells were given a pulse of photoirradiation that led to an immediate attenuation of cytotoxicity and a decrease in the release of IL-2 and IFN- γ compared with the nonirradiated group. The nonirradiated group showed a continuous increase in cytotoxicity and IL-2 and IFN- γ release, which plateaued overnight (Figure 4B). Subsequently, the resting CAR-T cells become reactivated upon resupplementation with folate-O-FITC, as manifested by the significant release of IL-2 and IFN- γ . Impressively, the cytotoxicity of the CAR-T cells even exceeded that of the nonirradiated cells 4 h after resupplementation, accompanied by a synchronous increase in IL-2 release that surpassed that in the nonirradiated group (Figure 4B). Concomitant with this progress was the formation, dispersion, and reformation of cellular aggregates (Figure 4C), and phenotypical changes serving as indicators of CAR-T cell activation, deactivation, and reactivation (Figure 4D), respectively. These observations correlated well with folate-O-FITC supplementation, UV irradiation,

and mediator resupplementation. Therefore, we concluded that CAR-T cells were able to shuttle between an activated and inert state by folate-O-FITC acting as a switch and a UV365 pulse acting as a regulator.

Spatial and Temporal Photoswitching of CAR-T Cells in FR-Positive Xenograft Tumor Models

Given the feasibility of this system *in vitro*, we next explored the possibility of the spatial and temporal photoswitching of CAR-T cells *in vivo*. We first examined the turn-on effect of folate-O-FITC using a diffuse SKOV3 tumor model (Song, et al., 2011). We found that SKOV3 is an FR-positive cell line that showed a weaker cytotoxic response to CAR-T cells than KB cells (Figures 5A and 5B), but could be easily transplanted into mice via intravenous injection. As anticipated, mice treated with high doses of the mediator exhibited significantly inhibited tumor proliferation compared with mice treated with a low dose of the mediator and mice not treated with the mediator (Figure 5C), indicating that the *in vivo* activation of CAR-T cells was successfully initiated by the mediator in a dose-dependent manner.

We next investigated the effects of the switchable regulation of CAR-T cells *in vivo*. To this end, we first evaluated the pharmacokinetics of the mediator after subcutaneous or intratumoral injection in healthy or KB tumor-bearing mice, respectively. The mediator was present in the circulation with pharmacokinetic properties, i.e., a half-life ($T_{1/2}$) of ~ 3 h and a mean retention time of ~ 4 h, comparable with those of its parental folate-FITC (Figures S5A and S5B), and it remained in the local tumor tissue for at least 12 h after a single intratumoral injection (Figure S5C). Moreover, the accessibility of percutaneous UV irradiation to the tumor burden was verified by *ex vivo* flow cytometry analyses (Figure S5D). These results suggest the feasibility and availability of evaluating the mediator in a tumor-bearing mouse model *in vivo*.

We then intratumorally injected KB tumor-bearing SCID/beige mice with an adequate number of CAR-T cells on day 0, followed by alternate-day dosing with the mediator. Inactivation was

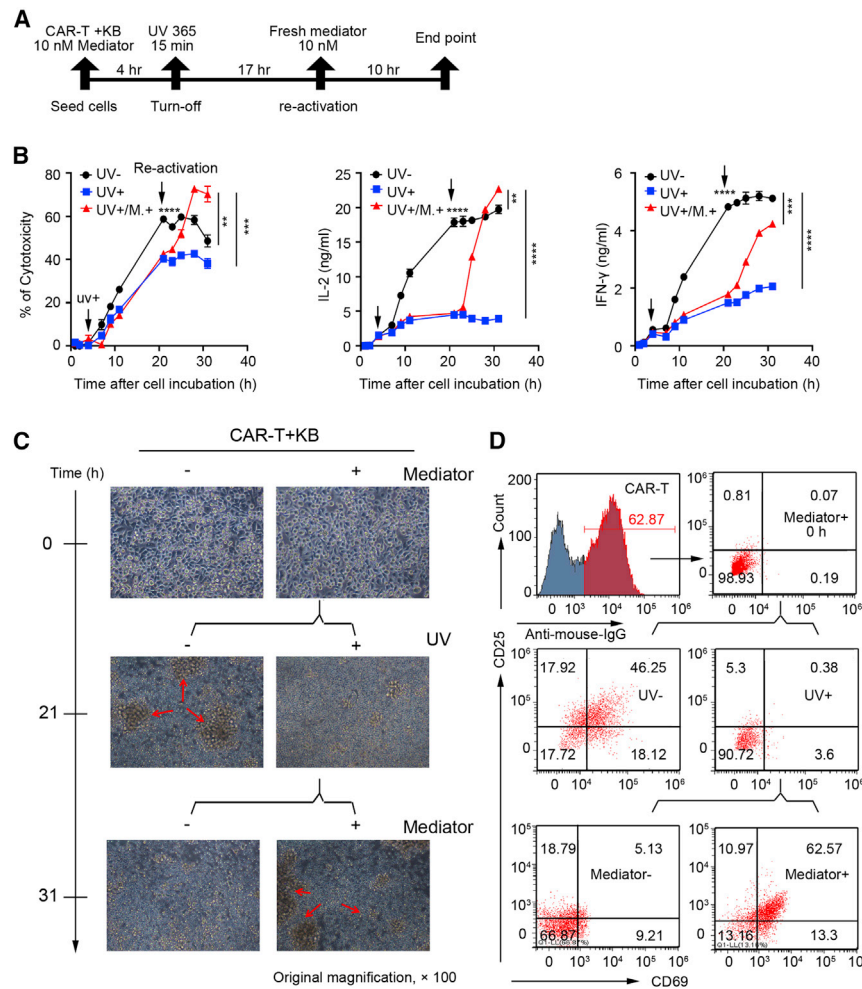


Figure 4. Time Course of CAR-T Cell Activation by Folate-O-FITC, Inactivation by Photoirradiation, and Reactivation by Folate-O-FITC Supplementation

(A) Flow chart of the *in vitro* analysis. CAR-T cells and KB cells were cocultured with the mediator at 0 h, and UV irradiation and reactivation were conducted at 4 and 21 h, respectively. The UV- group received the mediator at 0 h and no further treatment beyond that time; the UV+ group received the mediator at 0 h, UV irradiation at 4 h, and no further treatment beyond that time; and the UV+/M+ group received the mediator at 0 h, UV irradiation at 4 h, and another dose of the mediator at 21 h. (B) Quantification of LDH and cytokine (IFN- γ and IL-2) levels over time as described in (A). Data are presented as the mean \pm SEM derived from triplicate samples ($n = 3$). The p values shown were determined by two-tailed, unpaired Student's t tests, * $p \leq 0.05$, ** $p \leq 0.01$, *** $p \leq 0.001$, **** $p \leq 0.0001$.

(C) Microscopic images of CAR-T cells, including after activation by folate-O-FITC, inactivation by photoirradiation, and reactivation by folate-O-FITC supplementation, as described in (A and B). All images were acquired from the center field of each well and are shown at 100 \times magnification.

(D) Characterization of folate-O-FITC-mediated switchable regulation of CAR-T cells by flow cytometry analysis of CD25 and CD69 expression. CAR-T cells were cocultured with KB cells in the presence of the mediator and subsequently stained with anti-mouse-IgG F(ab) 2 antibody followed by anti-CD25 and anti-CD69 antibodies at the indicated times, as described in (C). The results represent findings from three independent experiments.

achieved by UV photoirradiation 6 h after each mediator injection on days 6, 8, and 10, and changes in both body weight and tumor growth were monitored for 2 weeks (Figure 6A). According to our results, the treatment of KB tumor-bearing mice with an adequate dose of CAR-T cells plus uninterrupted alternate-day doses of the mediator promoted rapid and continuous weight loss, suggesting the occurrence of cytokine-induced toxicity, and UV irradiation rapidly reversed such weight loss compared with those in the uninterrupted adapter-treated group. The continuing body weight loss was observed again upon resupplementation with the mediator (Figure 6B), implying the reactivation of CAR-T cells. These weight loss changes were correlated well with changes in cytokine production, as demonstrated by the related changes in the IFN- γ and IL-2 levels (Figure 6C). Notably, with the controllable cytokine secretion and rapid decrement in body weight loss, the integral antitumor effects were not compromised by this temporary switchable regulation (Figure 6D). These results are consistent with those of a parallel bioluminescence imaging (BLI) assay, in which photoirradiation treatment (Mediator+/UV+) led to obvious tumor growth relapse compared with mediator-only treatment (Mediator+/UV-) on day 10, while CAR-T cell reactivation and tumor inhibition were achieved again by reinjection of the mediator (Figures 6E–6G). Collectively, these results suggest that the cytokine-induced

toxicity of CAR-T cells can be regulated by transient cleavage of the mediator in a switchable manner without compromising antitumor activities.

DISCUSSION

CAR-T cell-based therapeutic approaches have improved in recent years but are still associated with significant safety and controllability issues. Numerous approaches have been implemented to address these issues, such as neutralizing inflammatory cytokines by antibodies, administering immunosuppressive drugs, and inducing CAR-T cell death via the suicide gene (Acharya, et al., 2019; Brentjens, et al., 2013; Lee, et al., 2014; Straathof, et al., 2005). Because all of these methods require the suppression of CAR-T activity, it is thus necessary to balance the benefits of suppressing CRS and inhibiting CAR-T cells in clinical applications. As the application of antagonist proteins, such as tocilizumab and anakinra, for blocking IL-6R and IL-1R (Giavridis, et al., 2018; Kotch, et al., 2019; Norelli, et al., 2018), respectively, can only be locked to known cytokines, the effect may not be sufficiently comprehensive to suppress CRS. Aiming to develop a feasible strategy to further enhance the controllability and safety of CAR-T cell technology, as a proof of concept, we report an approach using a photocleavable mediator and a

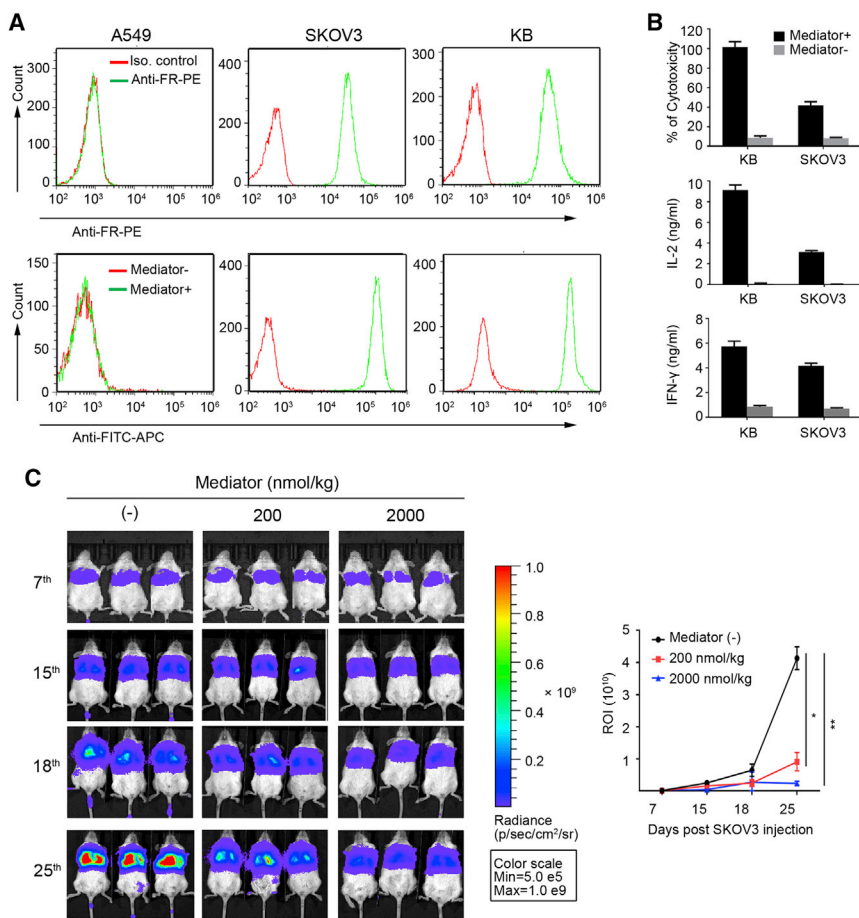


Figure 5. Folate-O-FITC-Mediated Activation of CAR-T Cells in Diffuse SKOV3 Tumor Xenografts

(A) Comparison of folate receptor expression on A549, KB, and SKOV3 cells using anti-FR-PE antibodies (top) and the mediator (bottom), respectively. Cells were first incubated with 10 nM mediator and then stained with anti-FITC-APC antibodies. The results shown represent the findings from three experiments.

(B) *In vitro* comparison of anti-FITC CAR-T cell responses with KB and SKOV3 cells. Anti-FITC CAR-T cells were cocultured for 24 h with KB or SKOV3 cells in the presence of 1 nM mediator at an E:T ratio of 20:1. Cells cultured without the mediator were used as a negative control. Cytotoxicity (top), IL-2 (middle), and IFN- γ (bottom) levels were measured and calculated as percentages. Data are presented as the mean \pm SEM derived from triplicate samples (n = 3).

(C) Time course of folate-O-FITC-mediated activation of CAR-T cells in diffuse SKOV3 tumor xenografts. Xenografts were monitored and quantitatively analyzed as regions of interest by BLI. NOG mice inoculated with luciferase-expressing SKOV3 cells were infused with 1×10^7 CAR-T cells; 7 days later, folate-O-FITC treatment, performed every other day, was executed six times at the indicated doses. Mice treated with high doses of the mediator achieved significant tumor growth inhibition. Data are presented as the mean \pm SEM derived from three mice per group (n = 3), the p values shown were determined by one-way ANOVA (Dunnett's multiple comparison test compared with mediator (-) treated group). *p \leq 0.05, **p \leq 0.01. The experiment was repeated three times with similar results, and one of three representative results is shown.

nondetrimental laser pulse that allows the regulation of CAR-T cells in a switchable manner at will, limiting the possible adverse effects without comprising the antitumor effects. Folate-FITC, with its conventional linker having been replaced with a UV-sensitive ortho-nitrobenzyl ester group, was adopted here because of its well-studied and successful application in the clinic (Lu, et al., 2009; Lu, et al., 2006; van Dam, et al., 2011).

We found that CAR-T cells were indeed highly cytotoxic to FR-positive cells only in the presence of the mediator and exhibited cytotoxic effects in a dose-dependent manner both *in vitro* and *in vivo*, verifying the specificity of the mediator for CAR-T cell activation. Furthermore, the cytotoxicity and cytokines release of CAR-T cells were rapidly inhibited upon photoirradiation, and reactivation of inactive CAR-T cells can be achieved by re-supplementation of mediator reversibly, addressing the inherent issues regarding the rapid and reversible control of CAR-T cells. Nevertheless, as *in vitro* assessment demonstrated in Figure 4, we found that the effects of UV-mediated detachment on cytotoxicity of CAR-T cells are compromised compared with those of cytokines release of CAR-T cells. The continuous persistence of cytotoxicity reflected by lactate dehydrogenase (LDH) might be explained by several factors, as LDH release might continue for a while, depending on renewal of the damaged plasma membrane, even when CAR-T cells are inactivated by photoirradiation. In addition, activated CAR-T cells might not be able to

convert to a resting state immediately upon exposure to a photoirradiation pulse because significantly lower levels of cytokines, such as IL-2 and IFN- γ , lasted for some time compared with those in the nonirradiated group. The persistent cytokines released into medium may also contribute to the release of LDH.

Whether this approach had the capacity to switchable regulation of CAR-T cells was evaluated using a xenograft model *in vivo*. KB cells were used because they express high levels of FR and can be easily implanted as solid tumors. According to our results, a body weight loss of \sim 10% was observed in tumor-bearing mice within 10 days of a single injection of an adequate dose of CAR-T cells plus uninterrupted alternate-day doses of the mediator, suggesting the occurrence of CRS (Lee, et al., 2019; Ma, et al., 2016). The potent decrement in cytokine-induced toxicity was rapidly promoted by simple UV irradiation, which broke the link between CAR-T cells and target cells, and CAR-T cell reactivation was achieved by supplementation with the mediator, enabling switchable regulation of the cytokine-induced toxicity of CAR-T cells. Although this demonstrated that the antitumor activity of CAR-T cells has not been significantly affected by such switchable regulation, the contrast of the tumor suppression effect of the CAR-T cells between "with mediator" and "without mediator" groups in Figure 6D is, to a lesser degree than that of previously reports using other

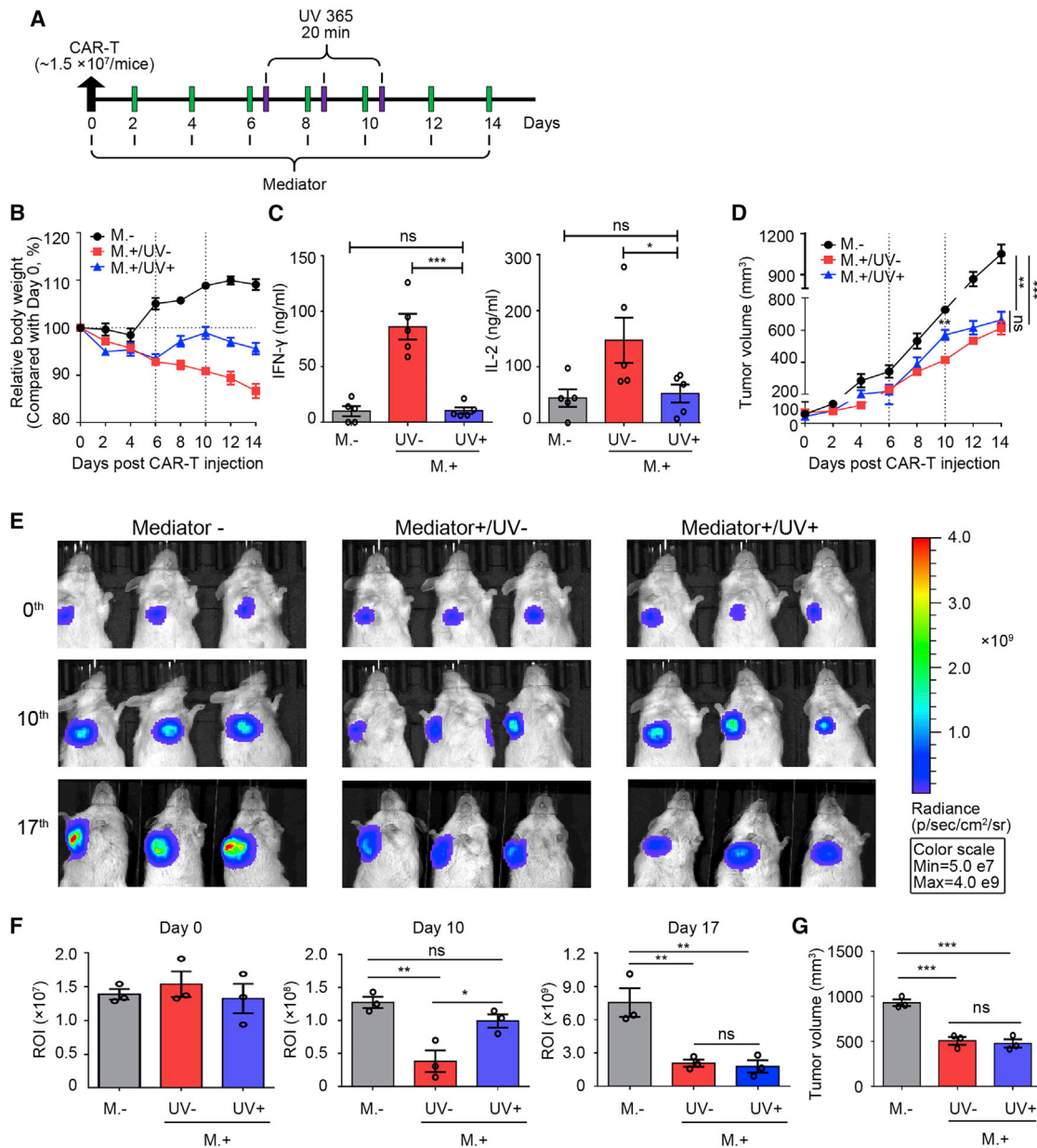


Figure 6. Verification of Photoswitchable CAR-T Cells in KB Tumor Xenograft Models

(A–F) Characterization of switchable regulation of CAR-T cell-mediated cytotoxicity *in vivo*. (A) Flow chart of the exploration of the *in vivo* activation and inactivation behavior of folate-O-FITC and photoirradiation, respectively. The KB tumor-bearing SCID/beige mice were intratumorally injected with 1.5×10^7 anti-FITC CAR-T cells on day 0, followed by alternate-day dosing with the mediator (500 nmol/kg). Changes in body weight and tumor growth were monitored alternately over 2 weeks. (B) Changes in body weight after administration of CAR-T cells in the absence (M–) or presence of the mediator (M+/UV–). Inactivation was achieved by UV photoirradiation 6 h after each mediator injection on days 6, 8, and 10 (M+/UV+), and reactivation was achieved by replenishing of mediator 4 h after each photoirradiation, respectively, as demonstrated in (A). (C) Analysis of IFN- γ and IL-2 secretion by CAR-T cells in plasma by ELISA on day 8. (D) The tumor growth after administration of CAR-T and mediator. For (B)–(D), data are presented as the mean \pm SEM derived from five mice per group ($n = 5$), and the p values shown were determined by two-tailed, unpaired Student’s t tests. Representative data from one of three experiments are shown and similar results were observed; (E) bioluminescence imaging and quantitative analyses of the region of interest (F) in mice inoculated with luciferase-transduced KB cells. (G) Measurement of body weight in g at the end of the study period (day 18). For (F) and (G), data are presented as the mean \pm SEM of three mice per group ($n = 3$), and p values shown were determined by two-tailed, unpaired Student’s t tests; * $p \leq 0.05$, ** $p \leq 0.01$, *** $p \leq 0.001$.

FR-positive cells, such as MDA-MB-231 cells (Lee, et al., 2019), and all groups of mice eventually succumbed to excessive tumor burden (data not show). The rapid growth and easy implantation

of KB cells are beneficial to the rapid assessment of the *in vivo* behavior of CAR-T cells, but also inevitably compromised their antitumor effects.

The use of bispecific adaptors to control CAR-T cell-derived toxicity has also been studied by other groups, and promising results have been generated (Kim, et al., 2015; Lee, et al., 2019; Ma, et al., 2016). Achieving rapid and flexible control of the toxicity of CAR-T cells, however, is still challenging due to the time-consuming procedures required for these adaptors, which generally include elaborate concentration and dosing schedules based on the metabolism and pharmacokinetics of the mediator (Lee, et al., 2019). The switchable CAR-T cells described here, which functioned intermittently under irradiation 6 h after each application of the mediator and were reactivated by resupplementation with the mediator 4 h after each irradiation, as described in Figure 6A, created a 44-h “active” duration and a 4-h “inactive” pulse within the 2-day interval; the effect in terms of overall antitumor activities was comparable with that of uninterrupted alternate-day dosing but was more beneficial in terms of tuning the toxicity of the CAR-T cells on demand. Given the high efficiency of UV-mediated cleavage, the active and inactive durations can be adjusted at will, regardless of the concentration and half-life of the mediator, which is a benefit of this approach. Nevertheless, cutting back on the dosage of the mediator but increasing the dosing frequency during the same time interval may have a similar effect but is beyond the scope of this study.

The versatile approach described here provides an appealing direction for clinical applications of photoswitchable CAR-T cells. There are, however, some limitations. One limitation is the wavelength of light: ~365 nm used in this study to perform photoswitching. The best wavelengths to trigger mediator cleavage are in the UV wavelength region, which is not medically useful due to its poor tissue penetration (less than a few millimeters) and its ability to induce DNA damage and mutations (Li and Chen, 2016). A series of photocleavable groups have emerged over the last decade to regulate bioactive molecules, and red and infrared light within wavelengths of ~650–950 nm may be optional choices because of less harm to living cells and the significant possibility for deeper tissue penetration (Papageorgiou, et al., 2000; Shanmugam, et al., 2016; Stolik, et al., 2000). Optimizations of the switchable parts, including but not limited to photocleavable groups, remain a topic of ongoing investigation, and become crucial to ensure this approach for clinical transformation. A variety of bioorthogonal cleavage reactions, including light-, chemical-, and enzyme-triggered reactions, have recently emerged (Li and Chen, 2016). The UV-photosensitive ortho-nitrobenzyl ester was selected as a linker in this study due to its high cleavability and rapid cleavage under biocompatible photoirradiation at 365 nm (Klan, et al., 2013; Li and Chen, 2016); these properties afford immediate and efficient detachment at the living cell level as needed. Given that the cleavage of mediators is not damaging to CAR-T cells, our results indicate that the control of CAR-T cells using a cleavable mediator is effective for reversing CRS without inhibiting the efficacy of CAR-T cell treatment, enabling the regulation of CAR-T cells in a switchable manner.

In conclusion, we report a platform that provides an instantaneous and recyclable methodology to enable the regulation of CAR-T cell activities in a flexible, on-and-off switchable manner. The spatial and temporal control of the toxicity of CAR-T cells under physiological conditions indicates the excellent biocompatibility of using such a triple-functional mediator as a molecular

switch. With the use of a light pulse, the mediator-based on-and-off switching of CAR-T cells at will may limit side effects without compromising antitumor effects, providing an attractive immunotherapeutic approach for overcoming some of the safety hurdles associated with current CAR-T cell-based therapies. Furthermore, with replacement of the folate moiety in the mediator with other ligands with a specific cell or tissue tropism, the photoswitchable CAR-T cells reported here may become a universal system that can be redirected against theoretically any antigen on the tumor surface. We believe that such a photoswitchable CAR-T cell system provides a direction for controllable immunotherapy and helps to increase the safety of CAR-T cells for future clinical applications.

SIGNIFICANCE

CAR-T is a powerful technology for cancer therapy, but is significantly limited by the safety issues because of the inability to flexibly control and terminate their activations. To this end, we developed an accurate and controllable approach based on a cleavable on-off mediator, where the bond-cleavage chemistry, i.e., photocleavable reaction, was combined with universal anti-FITC CAR-T cells. The activation of CAR-T cells strictly depended on the presence of the mediator and acted in a dose-dependent manner; also, the CAR-T-induced cytotoxicity can be rapidly terminated by the cleavage of the mediator, and the effects of CAR-T cells can be reactivated by the supplementation of the mediator without compromising therapeutic effects. This switchable approach was shown to be highly effective in the regulation of CAR-T cells both *in vitro* and *in vivo*. We believe that such a photoswitchable CAR-T system would pave a path for controllable immunotherapy and help to increase the safety of CAR-T for future clinical applications.

STAR★METHODS

Detailed methods are provided in the online version of this paper and include the following:

- KEY RESOURCES TABLE
- RESOURCE AVAILABILITY
 - Lead Contact
 - Materials Availability
 - Data and Code Availability
- EXPERIMENTAL MODELS AND SUBJECT DETAILS
 - Animals
 - Mammalian Cell Culture
- METHOD DETAILS
 - Detailed Synthetic Procedures to Folate-O-FITC (Compound 10)
 - Compound 1 1,4-Diazidobutane
 - Compound 2 4-azidobutan-1-amine
 - Compound 3 5-(3-(4-azidobutyl)thioureido)-2-(3,6-dihydroxy-9H-xanthen-9-yl) benzoic acid
 - Compound 4 1-(3-methoxy-4-(prop-2-yn-1-yloxy) phenyl) ethan-1-one

- Compound 5 1-(5-methoxy-2-nitro-4-(prop-2-yn-1-yloxy) phenyl) ethan-1-one
- Compound 6 1-(5-methoxy-2-nitro-4-(prop-2-yn-1-yloxy) phenyl) ethan-1-ol
- Compound 7 1-(5-methoxy-2-nitro-4-(prop-2-yn-1-yloxy) phenyl) ethyl (4-nitro phenyl) carbonate
- Compound 8 1-(5-methoxy-2-nitro-4-(prop-2-yn-1-yloxy) phenyl) ethyl (2-amino ethyl) carbamate
- Virus Production and Generation of CAR-Ts
- Evaluation of Transduction Efficiency and Function of CAR-Ts by Flow Cytometry Analysis
- Cytotoxicity and Cytokine Release Assay
- Photocleavage Experiments at the Cellular Level
- *In Vivo* Regulated Efficacy Assays

● QUANTIFICATION AND STATISTICAL ANALYSIS

SUPPLEMENTAL INFORMATION

Supplemental Information can be found online at <https://doi.org/10.1016/j.chembiol.2020.10.004>.

ACKNOWLEDGMENTS

We thank Mr. Sen Dou for his help in generating graphics. This work was supported by grants from the National Natural Science Foundation of China (81788101, 81630044, 81803419, 91753202, 21778015 and 81821004), the National Key Research and Development Program of China (2019ZX09739), Chinese Academy of Medical Science Innovation Fund for Medical Sciences (CIFMS 2017-12M-1-008, 2016-12M-1-003), and the PUMC Youth Fund (2017350001). All authors declare no competing financial interests. Additional data can be found in the supplementary materials.

AUTHOR CONTRIBUTIONS

B.Z., D.Z., and L.L. designed the study. B.Z., Y.W., S.H., Y.Y., and J.S. performed the experiments and analyzed the data. J.H., W.L., H.C., and W.S. helped to polish the language. W.M., S.L., and X.L. donated blood and contributed to the collection and assembly of data, data analysis, and interpretation. M.W., G.Z., and L.Z. provided comments. B.Z., X.Z., and D.Z. wrote the manuscript. All authors reviewed the manuscript.

DECLARATION OF INTERESTS

The authors declare no competing interests.

Received: August 7, 2020

Revised: September 7, 2020

Accepted: October 7, 2020

Published: October 27, 2020

REFERENCES

Acharya, U.H., Dhawale, T., Yun, S., Jacobson, C.A., Chavez, J.C., Ramos, J.D., Appelbaum, J., and Maloney, D.G. (2019). Management of cytokine release syndrome and neurotoxicity in chimeric antigen receptor (CAR) T cell therapy. *Expert Rev. Hematol.* **12**, 195–205.

Barrett, D.M., Singh, N., Porter, D.L., Grupp, S.A., and June, C.H. (2014). Chimeric antigen receptor therapy for cancer. *Annu. Rev. Med.* **65**, 333–347.

Brentjens, R.J., Davila, M.L., Riviere, I., Park, J., Wang, X., Cowell, L.G., Bartido, S., Stefanski, J., Taylor, C., Olszewska, M., et al. (2013). CD19-targeted T cells rapidly induce molecular remissions in adults with chemotherapy-refractory acute lymphoblastic leukemia. *Sci. Transl. Med.* **5**, 177ra138.

Brudno, J.N., and Kochenderfer, J.N. (2016). Toxicities of chimeric antigen receptor T cells: recognition and management. *Blood* **127**, 3321–3330.

Cao, Y., Rodgers, D.T., Du, J., Ahmad, I., Hampton, E.N., Ma, J.S., Mazagova, M., Choi, S.H., Yun, H.Y., Xiao, H., et al. (2016). Design of switchable chimeric antigen receptor T cells targeting breast cancer. *Angew. Chem. Int. Ed.* **55**, 7520–7524.

Chang, T.C., Adak, A.K., Lin, T.W., Li, P.J., Chen, Y.J., Lai, C.H., Liang, C.F., Chen, Y.J., and Lin, C.C. (2016). A photo-cleavable biotin affinity tag for the facile release of a photo-crosslinked carbohydrate-binding protein. *Bioorg. Med. Chem.* **24**, 1216–1224.

van Dam, G.M., Themelis, G., Crane, L.M., Harlaar, N.J., Pleijhuis, R.G., Kelder, W., Sarantopoulos, A., de Jong, J.S., Arts, H.J., van der Zee, A.G., et al. (2011). Intraoperative tumor-specific fluorescence imaging in ovarian cancer by folate receptor- α targeting: first in-human results. *Nat. Med.* **17**, 1315–1319.

Giavidris, T., van der Stegen, S.J.C., Eyquem, J., Hamieh, M., Piersigilli, A., and Sadelain, M. (2018). CAR T cell-induced cytokine release syndrome is mediated by macrophages and abated by IL-1 blockade. *Nat. Med.* **24**, 731–738.

Grupp, S.A., Kalos, M., Barrett, D., Aplenc, R., Porter, D.L., Rheingold, S.R., Teachey, D.T., Chew, A., Hauck, B., Wright, J.F., et al. (2013). Chimeric antigen receptor-modified T cells for acute lymphoid leukemia. *New Engl. J. Med.* **368**, 1509–1518.

Jung, M.E., Ouk, S., Yoo, D., Sawyers, C.L., Chen, C., Tran, C., and Wongvipat, J. (2010). Structure-activity relationship for thiohydantoin androgen receptor antagonists for castration-resistant prostate cancer (CRPC). *J. Med. Chem.* **53**, 2779–2796.

Kaneko, S., Nakayama, H., Yoshino, Y., Fushimi, D., Yamaguchi, K., Horiike, Y., and Nakanishi, J. (2011). Photocrosslinking of cell adhesion on amino-bearing surfaces by reversible conjugation of poly(ethylene glycol) via a photocleavable linker. *Phys. Chem. Chem. Phys.* **13**, 4051–4059.

Kim, M.S., Ma, J.S., Yun, H., Cao, Y., Kim, J.Y., Chi, V., Wang, D., Woods, A., Sherwood, L., Caballero, D., et al. (2015). Redirection of genetically engineered CAR-T cells using bifunctional small molecules. *J. Am. Chem. Soc.* **137**, 2832–2835.

Klan, P., Solomek, T., Bochet, C.G., Blanc, A., Givens, R., Rubina, M., Popik, V., Kostikov, A., and Wirz, J. (2013). Photoremovable protecting groups in chemistry and biology: reaction mechanisms and efficacy. *Chem. Rev.* **113**, 119–191.

Kotch, C., Barrett, D., and Teachey, D.T. (2019). Tocilizumab for the treatment of chimeric antigen receptor T cell-induced cytokine release syndrome. *Expert Rev. Clin. Immunol.* **15**, 813–822.

Lee, D.W., Gardner, R., Porter, D.L., Louis, C.U., Ahmed, N., Jensen, M., Grupp, S.A., and Mackall, C.L. (2014). Current concepts in the diagnosis and management of cytokine release syndrome. *Blood* **124**, 188–195.

Lee, Y.G., Chu, H., Lu, Y., Leamon, C.P., Srinivasarao, M., Putt, K.S., and Low, P.S. (2019). Regulation of CAR T cell-mediated cytokine release syndrome-like toxicity using low molecular weight adapters. *Nat. Commun.* **10**, 2681.

Li, J., and Chen, P.R. (2016). Development and application of bond cleavage reactions in bioorthogonal chemistry. *Nat. Chem. Biol.* **12**, 129–137.

Lu, Y., Xu, L.C., Parker, N., Westrick, E., Reddy, J.A., Vetzal, M., Low, P.S., and Leamon, C.P. (2006). Preclinical pharmacokinetics, tissue distribution, and antitumor activity of a folate-hapten conjugate-targeted immunotherapy in hapten-immunized mice. *Mol. Cancer Ther.* **5**, 3258–3267.

Lu, Y., Klein, P.J., Westrick, E., Xu, L.C., Santhapuram, H.K., Bloomfield, A., Howard, S.J., Vlahov, I.R., Ellis, P.R., Low, P.S., et al. (2009). Strategy to prevent drug-related hypersensitivity in folate-targeted hapten immunotherapy of cancer. *AAPS J.* **11**, 628–638.

Ma, J.S., Kim, J.Y., Kazane, S.A., Choi, S.H., Yun, H.Y., Kim, M.S., Rodgers, D.T., Pugh, H.M., Singer, O., Sun, S.B., et al. (2016). Versatile strategy for controlling the specificity and activity of engineered T cells. *Proc. Natl. Acad. Sci. U S A* **113**, E450–E458.

Menard-Moyon, C., Ali-Boucetta, H., Fabbro, C., Chaloin, O., Kostarelos, K., and Bianco, A. (2015). Controlled chemical derivatization of carbon nanotubes with imaging, targeting, and therapeutic capabilities. *Chemistry* **21**, 14886–14892.

- Midelfort, K.S., Hernandez, H.H., Lippow, S.M., Tidor, B., Drennan, C.L., and Witttrup, K.D. (2004). Substantial energetic improvement with minimal structural perturbation in a high affinity mutant antibody. *J. Mol. Biol.* **343**, 685–701.
- Norelli, M., Camisa, B., Barbiera, G., Falcone, L., Purevdorj, A., Genua, M., Sanvito, F., Ponzoni, M., Doglioni, C., Cristofori, P., et al. (2018). Monocyte-derived IL-1 and IL-6 are differentially required for cytokine-release syndrome and neurotoxicity due to CAR T cells. *Nat. Med.* **24**, 739–748.
- Oliveira, B.L., Stenton, B.J., Unnikrishnan, V.B., de Almeida, C.R., Conde, J., Negrao, M., Schneider, F.S.S., Cordeiro, C., Ferreira, M.G., Caramori, G.F., et al. (2020). Platinum-triggered bond-cleavage of pentynoyl amide and N-propargyl handles for drug-activation. *J. Am. Chem. Soc.* **142**, 10869–10880.
- Papageorgiou, P., Katsambas, A., and Chu, A. (2000). Phototherapy with blue (415 nm) and red (660 nm) light in the treatment of acne vulgaris. *Br. J. Dermatol.* **142**, 973–978.
- Sarfaty, M., Leshno, M., Gordon, N., Moore, A., Neiman, V., Rosenbaum, E., and Goldstein, D.A. (2018). Cost effectiveness of nivolumab in advanced renal cell carcinoma. *Eur. Urol.* **73**, 628–634.
- Schneider, C.A., Rasband, W.S., and Eliceiri, K.W. (2012). NIH Image to ImageJ: 25 years of image analysis. *Nat. Methods* **9**, 671–675.
- Shanmugam, S., Xu, J., and Boyer, C. (2016). Light-regulated polymerization under near-infrared/far-red irradiation catalyzed by bacteriochlorophyll a. *Angew. Chem. Int. Ed.* **55**, 1036–1040.
- Song, D.G., Ye, Q., Carpenito, C., Poussin, M., Wang, L.P., Ji, C., Figini, M., June, C.H., Coukos, G., and Powell, D.J., Jr. (2011). *In vivo* persistence, tumor localization, and antitumor activity of CAR-engineered T cells is enhanced by costimulatory signaling through CD137 (4-1BB). *Cancer Res.* **71**, 4617–4627.
- Di Stasi, A., Tey, S.K., Dotti, G., Fujita, Y., Kennedy-Nasser, A., Martinez, C., Straathof, K., Liu, E., Durett, A.G., Grilley, B., et al. (2011). Inducible apoptosis as a safety switch for adoptive cell therapy. *N. Engl. J. Med.* **365**, 1673–1683.
- Stolik, S., Delgado, J.A., Perez, A., and Anasagasti, L. (2000). Measurement of the penetration depths of red and near infrared light in human "ex vivo" tissues. *J. Photochem. Photobiol. B Biol.* **57**, 90–93.
- Straathof, K.C., Pule, M.A., Yotnda, P., Dotti, G., Vanin, E.F., Brenner, M.K., Heslop, H.E., Spencer, D.M., and Rooney, C.M. (2005). An inducible caspase 9 safety switch for T-cell therapy. *Blood* **105**, 4247–4254.
- Tamada, K., Geng, D., Sakoda, Y., Bansal, N., Srivastava, R., Li, Z., and Davila, E. (2012). Redirecting gene-modified T cells toward various cancer types using tagged antibodies. *Clin. Cancer Res.* **18**, 6436–6445.
- Tan, L.P., Wu, H., Yang, P.Y., Kalesh, K.A., Zhang, X., Hu, M., Srinivasan, R., and Yao, S.Q. (2009). High-throughput discovery of *Mycobacterium tuberculosis* protein tyrosine phosphatase B (MptpB) inhibitors using click chemistry. *Org. Lett.* **11**, 5102–5105.
- Tomlin, F.M., Gordon, C.G., Han, Y., Wu, T.S., Sletten, E.M., and Bertozzi, C.R. (2018). Site-specific incorporation of quadricyclane into a protein and photocleavage of the quadricyclane ligation adduct. *Bioorg. Med. Chem.* **26**, 5280–5290.
- Tso, K.K., Leung, K.K., Liu, H.W., and Lo, K.K. (2016). Photoactivatable cytotoxic agents derived from mitochondria-targeting luminescent iridium(III) poly(ethylene glycol) complexes modified with a nitrobenzyl linkage. *Chem. Commun.* **52**, 4557–4560.
- Urbanska, K., Lanitis, E., Poussin, M., Lynn, R.C., Gavin, B.P., Kelderman, S., Yu, J., Scholler, N., and Powell, D.J., Jr. (2012). A universal strategy for adoptive immunotherapy of cancer through use of a novel T-cell antigen receptor. *Cancer Res.* **72**, 1844–1852.
- Vaughan, T.J., Williams, A.J., Pritchard, K., Osbourn, J.K., Pope, A.R., Earnshaw, J.C., McCafferty, J., Hodits, R.A., Wilton, J., and Johnson, K.S. (1996). Human antibodies with sub-nanomolar affinities isolated from a large non-immunized phage display library. *Nat. Biotechnol.* **14**, 309–314.
- Wang, J., Liu, Y., Liu, Y., Zheng, S., Wang, X., Zhao, J., Yang, F., Zhang, G., Wang, C., and Chen, P.R. (2019). Time-resolved protein activation by proximal decaying in living systems. *Nature* **569**, 509–513.

STAR★METHODS

KEY RESOURCES TABLE

REAGENT or RESOURCE	SOURCE	IDENTIFIER
Antibodies		
Anti-Mouse IgG, F(ab') ₂ specific, Alexa Fluor 647	Jackson Immuno Research	Cat# 115-605-006; RRID: AB_2338903
Folic acid Antibody (FA1) [Alexa Fluor® 647]	Novus Biologicals	Cat# NB100-72975AF647; RRID: AB_2876876
Anti-FITC antibody (PE)	Abcam	Cat# 25539; RRID: AB_732396
Brilliant Violet 605 anti-human CD69	Biolegend	Cat# 310938; RRID: AB_2562307
PE anti-FOLR1 (Folate binding protein)	Biolegend	Cat# 908304; RRID: AB_2629795
PE anti-human CD25	Biolegend	Cat# 302606; RRID: AB_314276
APC anti-human CD3	Biolegend	Cat# 300412; RRID: AB_314066
Monoclonal Anti-FITC IgG-HRP Conjugate	Alpha Diagnostic International	Cat# 20376-HP; RRID: AB_2876877
Biological Samples		
Human PBMC, health donor	Peking Union Medical College Hospital	N/A
Chemicals, Peptides, and Recombinant Proteins		
Aim-V medium	Thermo	Cat# 12055091
RIMI 1640 Medium, no folic acid	Thermo	Cat# 27016-021
MEM, GlutaMAX Supplement	Thermo	Cat# 41090036
Dynabeads Untouched Human T Cells	Thermo	Cat# 11344D
Dynabeads Human T-expander CD3/CD28	Thermo	Cat# 11141D
Human IL-2 Recombinant Protein	Thermo	Cat# BMS334
Lipofectamine 3000 Transfection Reagent	Thermo	Cat# L3000015
Penicillin/streptomycin	Thermo	Cat# 15140163
Fetal Bovine Serum	Thermo	Cat# 16140071
Ficoll-Paque PLUS	GE Healthcare	Cat# 17-1440-02
7-Aminoactinomycin D	AAT Bioquest	Cat# 17501; CAS 7240-37-1
Compound Folate-FITC	(Kim, et al., 2015)	CAS 910661-33-5
4'-Hydroxy-3'-methoxyacetophenone	Macklin	Cat# H830242; CAS 498-02-2
Propargyl bromide	Macklin	Cat# P815876; CAS 106-96-7
Sodium borohydride	Aladdin	Cat# S108355; CAS 16940-66-2
4-Nitrophenyl Chloroformate	Aladdin	Cat# N159046; CAS 7693-46-1
Ethylenediamine	Aladdin	Cat# E112643; CAS 107-15-3
N-Hydroxysuccinimide	Macklin	Cat# N811124; CAS 6066-82-6
N,N'-Dicyclohexylcarbodiimide	Macklin	Cat# N806920; CAS 538-75-0
Folic acid	Macklin	Cat# F809516; CAS 59-30-3
Compound Folate-O-FITC, detailed synthesis described in Supplemental Information	This paper	N/A
Critical Commercial Assays		
CytoTox 96® Non-Radioactive Cytotoxicity Assay	Promega	Cat# G1780
Human IL-2 ELISA Kit	Dakewe	Cat# 1110202

(Continued on next page)

Continued

REAGENT or RESOURCE	SOURCE	IDENTIFIER
Human IFN- γ ELISA Kit	Dakewei	Cat# 1110002
Folic Acid (FA) ELISA kit	Alpha Diagnostic International	Cat# 0365-0B9
Oligonucleotides		
4m5.3 anti-FITC scFv	(Midelfort, et al., 2004)	N/A
4-1BB	Genebank	U03397.1
CD3 ζ	Genebank	J04132.1
Software and Algorithms		
Prism 6.0	Graphpad	https://www.graphpad.com/scientificsoftware/prism/
ChemDraw Professional 18.0	PerkinElmer	https://www.perkinelmer.com/category/chemdraw
CytExpert 2.3	Beckman Coulter	https://www.beckman.ae/flow-cytometry
ImageJ	(Schneider et al., 2012)	https://imagej.nih.gov/ij

RESOURCE AVAILABILITY

Lead Contact

Further information and requests for resources and reagents should be directed to and will be fulfilled by the lead contact, Xuan Zhang, MD (zxpumch@sina.com);

Materials Availability

This study did not generate any unique biological reagents. Synthesis of all chemicals is detailed within the manuscript.

Data and Code Availability

All data generated or analyzed during this study are included in this published article and its Supplementary Information files. The raw datasets supporting the current study have not been deposited in a public repository but are available from the corresponding author on request.

EXPERIMENTAL MODELS AND SUBJECT DETAILS

Animals

Six- to eight-week-old female SCID/beige or NOG mice (*Vital River Laboratory Animal Technology Co., Ltd. Beijing*) were maintained at Peking University Health Science Center in compliance with Peking University Institutional Animal Care and all studies reported here were approved by the Ethics Review Board of PUMC Hospital, Chinese Academy of Medical Science (CAMS). Mice were co-housed at 3-5 mice per cage and maintained on folic acid-deficient diet under pathogen-free conditions on a 12-h light cycle with access to food and water ad libitum.

Mammalian Cell Culture

All cells were maintained in a humidified incubator at 37C and 5% CO₂. KB cells were kindly provided by Prof. Xinjing Tang (Peking University) and maintained in RPMI 1640 medium (without folic acid) supplemented with 10% heat-inactivated fetal bovine serum (FBS) plus 1% antibiotics. The virus-producing cell line HEK293FT was purchased from Life Technologies (USA) and maintained in Dulbecco's modified Eagle's medium containing 10% FBS, 1% antibiotics, 0.1 mM MEM/nonessential amino acids, 1 mM sodium pyruvate, and 500 μ g/mL geneticin. Human CD3⁺ T cells were isolated from healthy volunteer donors by Ficoll-Pacque (Dakewei Biotech Co., Ltd.) and then subjected to negative selection (Life Technologies). All specimens were collected according to a protocol approved by the Institutional Review Board of our hospital. Isolated human T cells were subsequently cultured in Aim-V medium supplemented with 10% FBS and 300 IU/mL IL-2 (Life Technologies). Jurkat, A549 and SKOV3 cells were purchased from American Type Culture Collection (ATCC, Manassas, VA, USA) and cultured according to ATCC recommendations.

METHOD DETAILS

Detailed Synthetic Procedures to Folate-O-FITC (Compound 10)

The synthesis of the designed mediator molecule was based on a modular assembly as shown in [Figure S1](#). Briefly, the ortho-nitrobenzyl ester bearing a terminal alkyne and free amine group was obtained by propargylation, ester exchange, and ammonolysis from a commercial ortho-nitrobenzyl alcohol. Coupling of the ortho-nitrobenzyl ester to folate was conducted with DCC as the condensing reagent, and conjugation to FITC was then completed using the CuAAC reaction. ¹H NMR spectra were recorded on

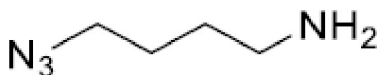
400 or 600 MHz using the residual solvent signal TMS as internal standard. Chemical shifts were reported in parts per million and coupling constants quoted in Hz. Matrix Assisted Laser Desorption/Ionization time-of-flight mass spectrometry with 2,5-Dihydroxybenzoic acid (DHB) as the matrix. MS were performed with Bruker BIFLEX III and Bruker Daltonics Autoflex speed MALDITOF/TOF. ^1H NMR, ^{13}C NMR data were recorded with an Avance 400/DPX (Bruker) and Avance III HD600 (Bruker). The more details about synthesis are described below:

Compound 1 1,4-Diazidobutane



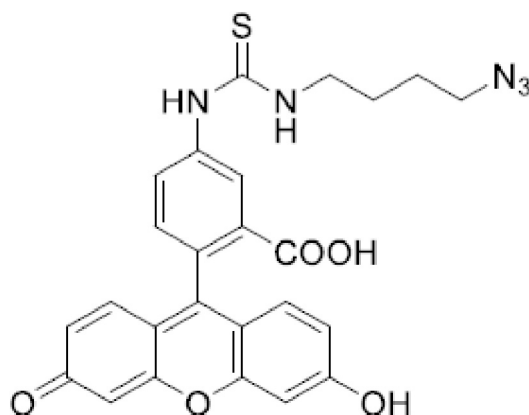
To a solution of 1,4-dibromobutane (2.38 mL, 20.0 mmol) in DMF (20 mL) was added a solution of NaN_3 (2.73 g, 42.0 mmol, 2.1 eq.) in H_2O (10 mL). After stirring overnight at 20°C , the reaction mixture was cooled down to room temperature and diluted with brine (40 mL) and hexanes (40 mL). The organic layer was separated and the aqueous layer was extracted with hexane (2×40 mL). The combined organic layers were dried over MgSO_4 , filtered and concentrated in vacuo to give title *compound 1* as clear oil (2.73 g, 19.6 mmol, 98%). ^1H NMR (400 MHz, CDCl_3) δ 3.30 (t, $J = 6.8$ Hz, 2H), 2.74 (t, $J = 6.7$ Hz, 2H), 1.70-1.60 (m, 2H), 1.53 (dt, $J = 14.2, 7.0$ Hz, 2H). Analytical data are in agreement with literature (Jung, et al., 2010).

Compound 2 4-azidobutan-1-amine



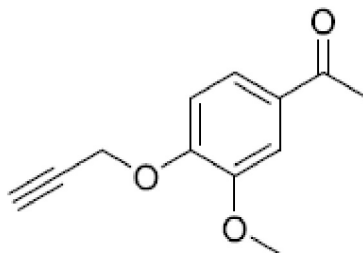
1,4-Diazidobutane (2.72 g, 19.4 mmol) was dissolved in a mixture of Et_2O (12 mL), EtOAc (12 mL) and aqueous HCl (1 M, 40 mL). Triphenylphosphine (5.09 g, 19.4 mmol, 1.00 eq.) was divided into several parts and added within 1 h at 0°C . The mixture was warmed to 21°C and stirred for an additional 20 hours. The aqueous layer was separated and washed with Et_2O (2×40 mL). The pH of the aqueous layer was adjusted to pH 13 with aqueous NaOH (2 M). After extraction with DCM (3×60 mL), the combined organic layers were dried over MgSO_4 , filtered and concentrated in vacuo to give title *compound 2* as clear oil (1.70 g, 77%). ^1H NMR (400 MHz, CDCl_3) δ 3.27 (t, $J = 6.8$ Hz, 2H), 2.71 (t, $J = 6.7$ Hz, 2H), 1.68-1.57 (m, 2H), 1.50 (dt, $J = 14.2, 7.0$ Hz, 2H). Analytical data are in agreement with literature (Jung, et al., 2010).

Compound 3 5-(3-(4-azidobutyl)thioureido)-2-(3,6-dihydroxy-9H-xanthen-9-yl) benzoic acid



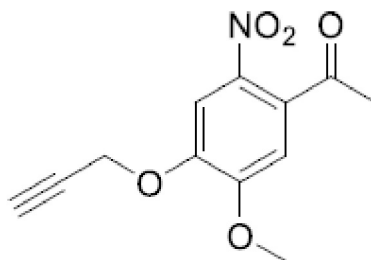
To a solution of 4-azidobutan-1-amine (34 mg, 0.3 mmol) in DMSO (5 mL) were added FITC (100 mg, 0.25 mmol) and DIPEA (65 mg, 0.5 mmol). After stirring for 6 hours. After the reaction was completed, the solvent was removed under vacuum, which also removed part of the excess 4-azidobutan-1-amine. The compound was purified by flash chromatography. The product was obtained as an orange solid in 40% yield. ^1H NMR (400 MHz, Methanol- d_4) δ 7.99 (s, 1H), 7.71-7.68 (m, 2H), 7.19 (d, $J = 8.0$ Hz, 1H), 7.12-7.10 (m, 2H), 6.64-6.60 (m, 4H), 3.69-3.65 (m, 2H), 3.37 (t, $J = 8.0$ Hz, 2H), 1.79-1.66 (m, 4H). ^{13}C NMR (151 MHz, Methanol- d_4) δ 182.3, 172.5, 157.4, 141.4, 137.5, 131.8, 130.6, 129.2, 119.2, 114.2, 103.7, 55.5, 52.0, 27.1. HRMS: m/z $\text{C}_{25}\text{H}_{21}\text{N}_5\text{NaO}_5\text{S}$ $[\text{M}+\text{Na}]^+$ 526.1156, Found 526.1160.

Compound 4 1-(3-methoxy-4-(prop-2-yn-1-yloxy) phenyl) ethan-1-one



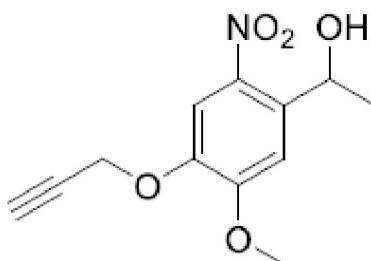
To a solution of 4-Methoxy-3-hydroxyacetophenone (3.32 g, 20.0 mmol) in DMF (20 mL) was added potassium carbonate (2.76 g, 20.0 mmol) and propargyl bromide (2.38 g, 20.0 mmol). The reaction mixture was stirred at room temperature for 2h. The reaction mixture was extracted with DCM (3×100 mL). The organic layer was dried over MgSO₄, filtered and concentrated in vacuo to give tile *compound 4* as a light brown solid (4.0 g, 98%). *Compound 4* ¹H NMR (600 MHz, CDCl₃) δ 7.57 (d, *J* = 8.4 Hz, 1H), 7.55 (s, 1H), 7.05 (d, *J* = 8.2 Hz, 1H), 4.84 (s, 2H), 3.93 (s, 3H), 2.57 (s, 3H). Analytical data are in agreement with literature (Tan, et al., 2009).

Compound 5 1-(5-methoxy-2-nitro-4-(prop-2-yn-1-yloxy) phenyl) ethan-1-one



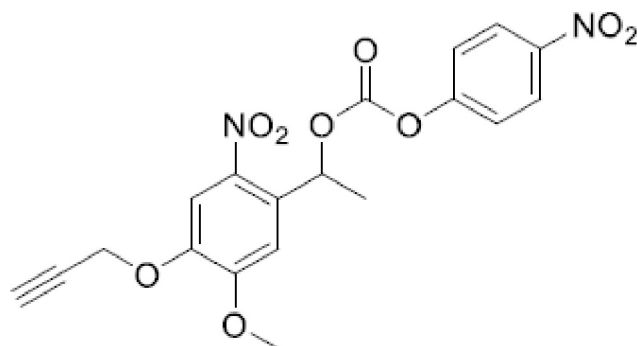
To a solution of 70% nitric acid (47 mL) and acetic anhydride (17 mL) was added dropwise a solution of *compound 4* (2.17 g, 8.20 mmol) dissolved in acetic anhydride (7 mL) at 0°C. The resultant yellow mixture was stirred for 3 h at room temperature. Cold deionized water (300 mL) was added to the mixture, which was then stirred for 2 h at 0°C. The yellow precipitate was collected by suction filtration and purified by column chromatography on silica gel. *Compound 5* was obtained as a yellow solid (1.45 g, 58%). *Compound 5* ¹H NMR (400 MHz, CDCl₃) δ 7.80 (s, 1H), 6.78 (s, 1H), 4.86 (s, 2H), 3.98 (s, 3H), 2.61 (s, 1H), 2.51 (s, 3H). Analytical data are in agreement with literature (Tso, et al., 2016).

Compound 6 1-(5-methoxy-2-nitro-4-(prop-2-yn-1-yloxy) phenyl) ethan-1-ol



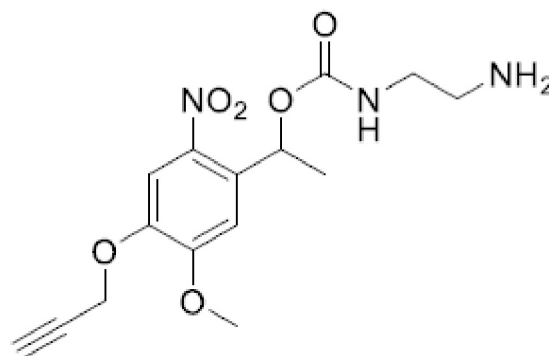
The solid *compound 5* (1.2 g, 4.9 mmol) was dissolved in THF/MeOH (20mL, 1/2, v/v) and cooled at 0°C for 5 min. Sodium borohydride (101 mg, 2.66 mmol) was added to the solution. The mixture was transferred to room temperature for 3 h. The reaction was quenched by deionized water (5 mL) and the pale-yellow crude product was extracted with CH₂Cl₂ (3×100 mL). The organic layers were concentrated by rotary evaporation and purified by column chromatography on silica gel. *Compound 6* was obtained as a yellow solid (1.11 g, 90%). *Compound 6* ¹H NMR (400 MHz, CDCl₃) δ 7.73 (s, 1H), 7.33 (s, 1H), 5.56 (q, *J* = 6.0 Hz, 1H), 4.80 (d, *J* = 2.4 Hz, 2H), 3.99 (s, 3H), 2.57 (t, *J* = 2.4 Hz, 1H), 1.55 (d, *J* = 6.4 Hz, 3H). Analytical data are in agreement with literature (Tso, et al., 2016).

Compound 7 1-(5-methoxy-2-nitro-4-(prop-2-yn-1-yloxy) phenyl) ethyl (4-nitro phenyl) carbonate



To a solution of *compound 6* (1.25 g, 5 mmol) in CH_3CN (5 ml) was added 4-nitrophenyl chloroformate (1.2 g, 6 mmol) and pyridine (5 mL) at 0°C . The mixture was stirred at room temperature for 6 h. The reaction was extracted with CH_2Cl_2 (3×100 mL). The organic layers were concentrated by rotary evaporation and purified by column chromatography on silica gel. *compound 7* was obtained as a light yellow solid (1.35 g, 65%). *Compound 7* ^1H NMR (400 MHz, CDCl_3) δ 8.24 (d, $J = 9.2$ Hz, 2H), 7.78 (s, 1H), 7.34 (d, $J = 9.2$ Hz, 2H), 7.15 (s, 1H), 6.54 (q, $J = 6.4$ Hz, 1H), 4.83 (d, $J = 2.0$ Hz, 2H), 4.02 (s, 3H), 2.60 (s, 1H), 1.77 (d, $J = 6.4$ Hz, 3H). ^{13}C NMR (151 MHz, CDCl_3) δ 155.32, 154.40, 151.46, 146.08, 145.43, 139.68, 132.40, 126.16, 125.32, 121.68, 115.67, 110.30, 108.32, 73.73, 57.02, 56.62, 22.01. HRMS: m/z $\text{C}_{19}\text{H}_{17}\text{N}_2\text{O}_9$ $[\text{M}+\text{H}]^+$ 417.0929, Found 417.0931.

Compound 8 1-(5-methoxy-2-nitro-4-(prop-2-yn-1-yloxy) phenyl) ethyl (2-amino ethyl) carbamate



To a solution of ethylenediamine (180 mg, 3 mmol) and DIPEA (623 μL , 4 mmol) in DCM (10 mL) were added dropwise a solution of *Compound 7* (832 mg, 2 mmol) in DCM (5 mL) at room temperature. After stirring at room temperature for overnight, the reaction mixture was concentrated to dryness in vacuo. The residue was purified using silica gel chromatography. *compound 8* was obtained as a yellow solid (566.7 mg, 84%). *Compound 8* ^1H NMR (400 MHz, CDCl_3) δ 7.75 (s, 1H), 7.04 (s, 1H), 6.38 (q, $J = 8.0$ Hz, 1H), 5.23 (s, 1H), 4.80 (d, $J = 4.0$ Hz, 2H), 3.96 (s, 3H), 3.23-3.15 (m, 2H), 2.81 (t, $J = 8.0$ Hz, 2H), 2.57 (t, $J = 4.0$ Hz, 1H), 1.60 (d, $J = 4.0$ Hz, 3H). ^{13}C NMR (151 MHz, CDCl_3) δ 155.67, 154.17, 145.42, 139.43, 135.13, 110.25, 108.46, 68.76, 56.97, 56.47, 53.49, 43.04, 41.38, 22.23. HRMS: m/z $\text{C}_{15}\text{H}_{20}\text{N}_3\text{O}_6$ $[\text{M}+\text{H}]^+$ 338.1347, Found 338.1352.

Compound 10 5-(3-(4-(4-((4-(1-(4-((2-amino-4-oxo-3,4-dihydropteridin-6-yl) methyl)amino)phenyl)-3-carboxy-1,6,11-trioxo-12-oxa-2,7,10-triazatetradecan-13-yl)-2-methoxy-5nitrophenoxy)methyl)-1H-1,2,3-triazol-1-yl)butyl)thioureido)-2-(6-hydroxy-3-oxo-3H-xanthen-9-yl) benzoic acid

A solution of folic acid (302 mg, 0.68 mmol), NHS (86 mg, 0.75 eq.), and dicyclohexylcarbo-diimide (DCC) (154 mg, 0.75 eq.) in anhydrous DMSO (16 mL) was stirred for 4 h in the dark. The reaction mixture was filtered over a PTFE (0.45 μm) membrane to remove dicyclohexylurea. *Compound 8* (229 mg 0.68 mmol) were added to the filtrate. The reaction mixture was stirred for 2 days in the dark. The clear solution was then concentrated by partial removal of the solvent under reduced pressure at 40°C . The solution was poured into a cold solution of acetone/diethyl ether (30:70% v/v ratio) resulting in precipitation of the product. The obtained precipitate was washed with 50 mL of acetone/diethyl ether solution (30:70% v/v ratio) and diethyl ether (3×50 mL) to remove traces of unreacted reagents and DIPEA-NHS salt. The product was dried in vacuum over P_2O_5 overnight (310 mg, 60%). The *compound 9* was direct used for the following click reactions without further purifications. To a solution of *compound 9* (343 mg, 0.68 mmol) in DMSO (10 mL) was added *compound 3* (343 mg, 0.68 mmol), $\text{CuSO}_4 \cdot 5\text{H}_2\text{O}$ (17 mg, 0.068 mmol) and Sodium L-Ascorbate (54 mg, 0.272 mmol)

under nitrogen atmosphere. The reaction was stirred at room temperature for 2 days. The solution was poured into a cold solution of acetone/diethyl ether (30:70% v/v ratio) resulting in precipitation of the product. The obtained precipitate was washed with DCM (50 mL) and water (50 mL). The product was purified by HPLC and freeze-drying to give *compound 10* as a yellow solid (395.4 mg, 41%). ¹H NMR (600 MHz, DMSO) δ 8.63 (s, 1H), 8.38–8.08 (m, 2H), 7.99–7.76 (m, 2H), 7.75–7.52 (m, 2H), 7.42–7.28 (d, *J* = 6.0 Hz, 1H), 7.28–7.13 (m, 1H), 7.11–7.04 (m, 1H), 6.98–6.81 (s, 2H), 6.71–6.52 (m, 5H), 6.18–5.98 (s, 1H), 5.32–5.13 (m, 2H), 4.62–4.30 (m, 4H), 3.97–3.68 (m, 3H), 3.04–2.91 (m, 5H), 2.16–2.07 (s, 1H), 2.06–1.69 (m, 4H), 1.52–1.46 (s, 6H). MALDI-TOF-MS: *m/z* C59H57N15NaO16S [M+Na]⁺ 1286.37, Found 1286.85; C59H57KN15O16S [M+K]⁺ 1302.35, Found 1302.83.

Virus Production and Generation of CAR-Ts

A gene cassette containing the 4M5.3 anti-FITC scFv (Ma, et al., 2016; Midelfort, et al., 2004; Vaughan, et al., 1996), the CD8 α hinge and transmembrane region, and the cytoplasmic domains of 4-1BB and CD3 ζ was synthesized by Icartab Co., Ltd. (SuZhou, China) and cloned into a lentivirus vector. Lentivirus production and transduction of human T cells were performed as previously described (Kim, et al., 2015; Ma, et al., 2016). Briefly, HEK293FT cells were transfected with the anti-FITC CAR, pspax2, and pMD2.g plasmids using Lipofectamine 3000 (Life Technologies). The medium was changed 6 h after transfection, and the viral supernatant was harvested 48 h after transfection. Viral particles were concentrated 30-fold by ultracentrifugation for 2 h at 25,000 rpm with a Beckman Ti70 rotor (Beckman Coulter) and frozen at –80°C until ready for use. Human T cells were purified from peripheral blood mononuclear cells using a Dynabead Untouched Human T cells kit (Life Technologies) and further activated for 24 h with CD3/CD28-coated magnetic beads (Life Technologies) before infection. Concentrated lentivirus was then applied to activated human T cells (~50 μ L/10⁶ human T cells in 24-well culture plates) in the presence of 10 μ g/mL polybrene and 50 IU/mL IL-2 and centrifuged at 1000 \times *g* for 2 h at 32°C. The next day, viral supernatants were replaced with fresh medium containing 300 IU/mL IL-2, and the transduced T cells were maintained at 0.5 \times 10⁶ cells/mL in complete growth medium, which was replenished every 4 days.

Evaluation of Transduction Efficiency and Function of CAR-Ts by Flow Cytometry Analysis

The transduction efficiency and function of CAR-Ts were both verified by flow cytometry, as previously described (Kim, et al., 2015). Briefly, to assess anti-FITC CAR expression, CAR-Ts were incubated with APC-conjugated anti-mouse IgG F(ab')² antibodies for 1 h at 4°C and then analyzed using a CytoFLEX flow cytometer (Beckman Coulter, Inc.). To determine the availability of the folate-based mediator, CAR-Ts were stained with the mediator and APC-conjugated anti-mouse IgG F(ab')² antibodies simultaneously, and the binding capacity of FITC was measured based on the percentage of cell clusters positive for both FITC and APC. The affinity of KB cells for the mediator was verified by incubation of KB cells with 10 nM mediator for 1 h at room temperature, followed by staining with an anti-FITC antibody conjugated to a PE dye (Abcam, Cambridge, UK) for more than 45 min. After being washed twice, the cells were analyzed using a CytoFLEX flow cytometer.

Cytotoxicity and Cytokine Release Assay

KB cells were mixed with anti-FITC CAR-Ts at an E:T ratio of 10:1 in 200 μ L of folate-deficient medium with different concentrations of mediator for 24 – 48 h. Cytolytic activity was determined using a lactate dehydrogenase-based (LDH) method with a CytoTox 96 Nonradioactive Cytotoxicity Assay kit (Promega, Madison, WI, USA) following the manufacturer's protocol. The percent cytotoxicity was calculated as follows: % cytotoxicity = ((experimental – effector spontaneous – target spontaneous) / (target maximum – target spontaneous)) \times 100. The remaining culture supernatants were harvested and assayed for the presence of IFN- γ and IL-2 using an enzyme-linked immunosorbent assay kit (Dakewei Biotech Co., Ltd.), according to the manufacturer's instructions.

Photocleavage Experiments at the Cellular Level

For cleavage assays, KB cells were incubated with 100 nM mediator for 1 h at room temperature and then washed twice with wash buffer (PBS + 3% bovine serum albumin) to remove excess mediator. Cells were resuspended in 200 μ L PBS at 1 \times 10⁶ cells/mL and then subjected to UV irradiation at 365 nm approximately 5 cm above the cell surface using a UV lamp (15 W \times 16, UV lamp power: 2.76 mW/cm²; Panchum, photochemical reactor PR-2000) for 20 min at room temperature. A control sample was not subjected to photoirradiation. After UV irradiation, the cleaved part of the mediator was removed from reactions by a series of three washes. The cleavage of CAR-Ts was similar to that of KB cells, except that the CAR-Ts were first stained with the mediator and then stained with an anti-folate antibody (Novus Biologicals) conjugated to an Alexa Fluor 647 dye. The cleavage efficiency of the mediator was determined by the attenuation of the fluorescent signal as determined by flow cytometry analysis. Additionally, the viability of cells after UV irradiation was confirmed by flow cytometry analysis using both the 7-AAD and trypan blue methods.

For immunofluorescent imaging, CAR-Ts and KB cells were stained with anti-CD3-APC and anti-FR-PE antibodies, respectively, and cocultured in the presence or absence of the mediator at a ratio of 1:1 for 1 h at 4°C. After three washes with PBS, some of the mediator-treated cells were subjected to UV irradiation (365 nm) for 20 min and then washed adequately to remove the cleaved mediator. The remaining mediator-treated cells were used as a non-photoirradiated control and were subjected to the same washing process as the photoirradiation group. Analyses were performed using Amnis IDEAS software to evaluate the binding and separation of CAR-Ts and KB cells mediated by the mediator. All images were acquired using a 40 \times objective (ImageStream x, Amnis), analyzed using IDEAS software (Amnis), and illustrated with a channel series, including Bright field mode (BF, channel 1). The fluorescence channels used for imaging KB and CAR-T cells were channel 2 (PE, anti-FR-PE) and channel 3 (APC, anti-mouse-IgG F(ab')²-APC), respectively.

In Vivo Regulated Efficacy Assays

To evaluate the effects of the regulation of CAR-T cells *in vivo*, a KB tumour-bearing SCID/beige mouse model was applied as previously described with slight changes (Lee, et al., 2019). Briefly, immunodeficient SCID/beige mice (6–8 weeks of age, Vital River Laboratory Animal Technology Co., Ltd., Beijing) were implanted subcutaneously with 1×10^7 KB cells and received an intratumoural injection of $1.5\text{--}2 \times 10^7$ anti-FITC CAR-T cells when the tumour reached $\sim 100 \text{ mm}^3$ in size on day 0. Alternate-day dosing with the mediator was applied starting on this day, and inactivation was achieved by UV photoradiation 6 h after each mediator injection on days 6, 8 and 10 ($\sim 5 \text{ cm}$ from the skin for 5 min using a 3 W flashlight). Mouse blood was also collected to measure the levels of IL-2 and IFN- γ using ELISA (BioLegend, CA), and CAR-T cell-induced toxicity was monitored by measuring body weight loss. The tumour dimensions were measured with callipers, and the tumour volume was calculated using the following formula: volume = (length \times width²)/2, in which the length was the greatest longitudinal diameter, and the width was greatest transverse diameter. For the diffuse tumour model, female NOD.Cg-Prkdc^{scid}Il2rg^{tm1Sug}/Jicrl mice (NOG mice; 6–8 weeks of age) were intravenously inoculated with 2×10^6 SKOV3 cells transfected with luciferase, and engraftment was confirmed by BLI 1 week later. The next day, CAR-T cells were infused intravenously (1×10^7 cells/per mouse) and treated with the indicated amounts of the mediator. In parallel, mice in control groups were injected with only CAR-T cells. Tumour growth was monitored weekly by BLI.

QUANTIFICATION AND STATISTICAL ANALYSIS

All statistical calculations were performed using GraphPad Prism 6. Accordingly, data sets were subjected to one-way ANOVA (Dunnett's multiple comparison) and the two-tailed unpaired Student's t-test as indicated in the figures. A p values less than 0.05 were considered significant. * $p \leq 0.05$, ** $p \leq 0.01$, *** $p \leq 0.001$, **** $p \leq 0.0001$. Sample sizes are indicated in the respective figure legend.